

基于2-2型压电复合材料的新型宽频带径向振动超声换能器

陈诚 林书玉

A new broadband radial vibration ultrasonic transducer based on 2-2 piezoelectric composite material

Chen Cheng Lin Shu-Yu

引用信息 Citation: *Acta Physica Sinica*, 70, 017701 (2021) DOI: 10.7498/aps.70.20201352

在线阅读 View online: <https://doi.org/10.7498/aps.70.20201352>

当期内容 View table of contents: <http://wulixb.iphy.ac.cn>

您可能感兴趣的其他文章

Articles you may be interested in

半导体激光器输出混沌光的延时特性和带宽

Time delay characteristics and bandwidth of chaotic laser from semiconductor laser

物理学报. 2018, 67(14): 140501 <https://doi.org/10.7498/aps.67.20180035>

混沌光注入垂直腔面发射激光器混沌输出的时延和带宽特性

Performances of time-delay signature and bandwidth of the chaos generated by a vertical-cavity surface-emitting laser under chaotic optical injection

物理学报. 2017, 66(24): 244206 <https://doi.org/10.7498/aps.66.244206>

高斯切趾型光纤布拉格光栅外腔半导体激光器的混沌输出特性

Characteristics of chaotic output from a Gaussian apodized fiber Bragg grating external-cavity semiconductor laser

物理学报. 2017, 66(24): 244207 <https://doi.org/10.7498/aps.66.244207>

基于拓扑优化设计的宽频吸波复合材料

Broadband absorbent materials based on topology optimization design

物理学报. 2018, 67(21): 217801 <https://doi.org/10.7498/aps.67.20181170>

引入界面耦合系数的长片型磁电层状复合材料的等效电路模型

Equivalent circuit model for plate-type magnetoelectric laminate composite considering an interface coupling factor

物理学报. 2018, 67(2): 027501 <https://doi.org/10.7498/aps.67.20172080>

半导体激光器混沌输出的延时特征和带宽

Time delay signature and bandwidth of chaotic laser output from semiconductor laser

物理学报. 2020, 69(9): 090501 <https://doi.org/10.7498/aps.69.20191881>

基于 2-2 型压电复合材料的新型宽频带 径向振动超声换能器*

陈诚 林书玉†

(陕西师范大学, 陕西省超声学重点实验室, 西安 710119)

(2020 年 8 月 17 日收到; 2020 年 9 月 3 日收到修改稿)

本文提出了一种基于 2-2 型压电复合材料的新型宽频带径向振动超声换能器, 它主要由内金属圆环和外压电陶瓷复合材料圆环组成. 首先利用 Newnham 串并联理论和均匀场理论推导了 2-2 型压电复合材料的等效参数; 其次利用解析法得到了金属圆环和径向极化压电陶瓷圆环径向振动的机电等效电路; 最后得到了换能器的六端机电等效电路, 从而得到了换能器的频率方程. 接着分析了换能器共振频率和反共振频率以及有效机电耦合系数与几何尺寸、两相体积占比的关系, 采用仿真软件对新型换能器的径向振动进行了数值模拟. 结果表明, 利用解析法得到的共振频率和反共振频率与数值模拟结果吻合较好. 此外, 对换能器在水下的辐射声场进行了仿真研究, 结果表明新型复合材料径向换能器相比传统纯陶瓷径向换能器, 发射电压响应幅值更大, 工作带宽提高接近一倍, 声匹配更佳.

关键词: 复合材料等效参数, 径向振动, 带宽, 声匹配

PACS: 77.84.Lf, 43.38.+n, 43.30.+m

DOI: 10.7498/aps.70.20201352

1 引言

径向振动换能器具有辐射面积大、辐射效率高、径向辐射均匀, 作用范围广等优点, 因此被广泛应用于水声、超声降解以及声化学等超声液体处理技术领域^[1]. 径向换能器种类主要有以下几种: 圆管型压电陶瓷换能器^[2]、复合型圆管压电换能器^[3]和径向复合压电超声换能器等^[4,5]. 另一方面, 2-2 型压电复合材料是现在研究最具体、发展前景最好的压电复合材料之一. 这种新型材料相较于传统纯压电陶瓷, 具有低阻抗、低机械品质因数、频带宽等优点^[6,7].

本文提出了一种基于 2-2 型压电复合材料的新型径向振动超声换能器, 如图 1 所示, 它是由内金属圆环和外压电复合陶瓷圆环组成. 首先推导

了 2-2 型压电复合材料的等效参数, 并利用解析法推导了金属圆环和径向极化压电陶瓷复合材料圆环径向振动的机电等效电路和换能器的频率方程. 接着采用仿真软件对新型换能器的径向振动性能进行数值仿真模拟, 并对结果进行分析. 最后研究了新型径向换能器较传统径向纯陶瓷换能器在工作带宽和声匹配上的性能提升.

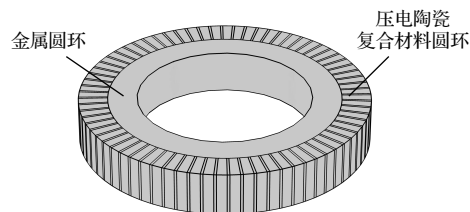


图 1 新型径向振动复合材料圆环换能器
Fig. 1. New radial vibration composite ring transducer.

* 国家自然科学基金 (批准号: 11674206, 11874253) 资助的课题.

† 通信作者. E-mail: sylin@snnu.edu.cn

2 2-2 型压电复合材料等效参数推导

如图 2 所示, 取 z 方向为极化方向, 压电相为横观各向同性体, 聚合物相为各向同性体, 聚合物相无压电效应。

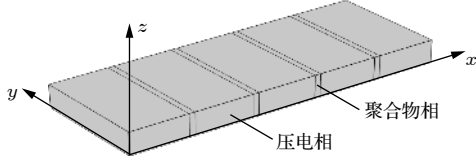


图 2 2-2 型压电复合材料
Fig. 2. 2-2 piezoelectric composite.

压电相本构关系为 [8,9]

$$\begin{bmatrix} T_1^c \\ T_2^c \\ T_3^c \\ T_4^c \\ T_5^c \\ T_6^c \end{bmatrix} = \begin{bmatrix} C_{11}^c & C_{12}^c & C_{13}^c & 0 & 0 & 0 \\ C_{12}^c & C_{11}^c & C_{13}^c & 0 & 0 & 0 \\ C_{13}^c & C_{13}^c & C_{33}^c & 0 & 0 & 0 \\ 0 & 0 & 0 & C_{44}^c & 0 & 0 \\ 0 & 0 & 0 & 0 & C_{44}^c & 0 \\ 0 & 0 & 0 & 0 & 0 & C_{66}^c \end{bmatrix} \times \begin{bmatrix} S_1^c \\ S_2^c \\ S_3^c \\ S_4^c \\ S_5^c \\ S_6^c \end{bmatrix} - \begin{bmatrix} 0 & 0 & e_{31} \\ 0 & 0 & e_{31} \\ 0 & 0 & e_{33} \\ 0 & e_{15} & 0 \\ e_{15} & 0 & 0 \\ 0 & 0 & 0 \end{bmatrix} \times \begin{bmatrix} E_1^c \\ E_2^c \\ E_3^c \end{bmatrix}, \quad (1)$$

$$\begin{bmatrix} D_1^c \\ D_2^c \\ D_3^c \end{bmatrix} = \begin{bmatrix} 0 & 0 & 0 & 0 & e_{15} & 0 \\ 0 & 0 & 0 & e_{15} & 0 & 0 \\ e_{31} & e_{31} & e_{33} & 0 & 0 & 0 \end{bmatrix} \times \begin{bmatrix} S_1^c \\ S_2^c \\ S_3^c \\ S_4^c \\ S_5^c \\ S_6^c \end{bmatrix} + \begin{bmatrix} \varepsilon_{11}^c & 0 & 0 \\ 0 & \varepsilon_{11}^c & 0 \\ 0 & 0 & \varepsilon_{33}^c \end{bmatrix} \times \begin{bmatrix} E_1^c \\ E_2^c \\ E_3^c \end{bmatrix}, \quad (2)$$

其中 T_i^c ($i=1, 2, 3, \dots, 6$) 为应力, S_i^c ($i=1, 2, 3, \dots, 6$) 为应变, E_i^c ($i=1, 2, 3$) 为电场强度分量, D_i^c ($i=1, 2, 3$) 为电位移分量, C_{ij}^c ($i, j=1, 2, 3, \dots, 6$) 为常电场刚度系数, e_{ij}^c ($i, j=1, 2, 3, \dots, 6$) 为常应变压电应力

系数, ε_{ij}^c ($i, j=1, 2, 3$) 为常应变介电系数, 上标 c 代表压电相, 上标 p 代表聚合物相, 上标 cp 代表复合材料。

聚合物相本构关系为

$$\begin{bmatrix} T_1^p \\ T_2^p \\ T_3^p \\ T_4^p \\ T_5^p \\ T_6^p \end{bmatrix} = \begin{bmatrix} C_{11}^p & C_{12}^p & C_{12}^p & 0 & 0 & 0 \\ C_{12}^p & C_{11}^p & C_{12}^p & 0 & 0 & 0 \\ C_{12}^p & C_{12}^p & C_{11}^p & 0 & 0 & 0 \\ 0 & 0 & 0 & C_{66}^p & 0 & 0 \\ 0 & 0 & 0 & 0 & C_{66}^p & 0 \\ 0 & 0 & 0 & 0 & 0 & C_{66}^p \end{bmatrix} \times \begin{bmatrix} S_1^p \\ S_2^p \\ S_3^p \\ S_4^p \\ S_5^p \\ S_6^p \end{bmatrix}, \quad (3)$$

$$\begin{bmatrix} D_1^p \\ D_2^p \\ D_3^p \end{bmatrix} = \begin{bmatrix} \varepsilon_{11}^p & 0 & 0 \\ 0 & \varepsilon_{11}^p & 0 \\ 0 & 0 & \varepsilon_{11}^p \end{bmatrix} \times \begin{bmatrix} E_1^p \\ E_2^p \\ E_3^p \end{bmatrix}. \quad (4)$$

该复合材料主向 (z 方向) 拉伸时, 不会引起剪切变形的耦合效应, 故可将 $T_4 = T_5 = T_6 = 0$, $E_1 = E_2 = 0$ 处理, 根据 Newnham 串并联理论 [10] 可以写出各个方向应力和应变关系式, 其中 v_c 代表压电相体积分数, v_p 代表聚合物相体积分数, $v_c + v_p = 1$ 。

在 x 方向, 压电相和聚合物相串联, 则各相应力相等, 应变为各相应应变之和, 即:

$$T_1^{cp} = T_1^c = T_1^p, \quad S_1^{cp} = v_c S_1^c + v_p S_1^p. \quad (5)$$

在 y 方向, 压电相和聚合物相并联, 则各相应变相等, 应力为各相应应力之和, 即:

$$T_2^{cp} = v_c T_2^c + v_p T_2^p, \quad S_2^{cp} = S_2^c = S_2^p. \quad (6)$$

在 z 方向, 压电相和聚合物相并联, 则各相应变相等, 应力为各相应应力之和, 电场强度分量相等, 电位移分量为各相电位移分量之和即:

$$T_3^{cp} = v_c T_3^c + v_p T_3^p, \quad S_3^{cp} = S_3^c = S_3^p, \\ E_3^{cp} = E_3^c = E_3^p, \quad D_3^{cp} = v_c D_3^c + v_p D_3^p. \quad (7)$$

取两相中相等的场量作为独立变量建立本构关系 [11], 在压电相中, 取 T_1^c , S_2^c , S_3^c , E_3^c 为独立变量, 本构方程可表示为

$$\begin{bmatrix} S_1^c \\ T_2^c \\ T_3^c \\ D_3^c \end{bmatrix} = A^c \times \begin{bmatrix} T_1^c \\ S_2^c \\ S_3^c \\ E_3^c \end{bmatrix}, \quad (8)$$

$$A^c = \begin{bmatrix} \frac{1}{C_{11}^c} & -\frac{C_{12}^c}{C_{11}^c} & -\frac{C_{13}^c}{C_{11}^c} & \frac{e_{31}^c}{C_{11}^c} \\ \frac{C_{12}^c}{C_{11}^c} & C_{11}^c - \frac{C_{12}^c{}^2}{C_{11}^c} & C_{13}^c - \frac{C_{12}^c C_{13}^c}{C_{11}^c} & \frac{C_{12}^c}{C_{11}^c} e_{31}^c - e_{31}^c \\ \frac{C_{13}^c}{C_{11}^c} & C_{13}^c - \frac{C_{12}^c C_{13}^c}{C_{11}^c} & C_{33}^c - \frac{C_{13}^c{}^2}{C_{11}^c} & \frac{C_{13}^c}{C_{11}^c} e_{31}^c - e_{33}^c \\ \frac{e_{31}^c}{C_{11}^c} & e_{31}^c - \frac{C_{12}^c}{C_{11}^c} e_{31}^c & e_{33}^c - \frac{C_{13}^c}{C_{11}^c} e_{31}^c & \frac{e_{31}^c{}^2}{C_{11}^c} + \varepsilon_{33}^c \end{bmatrix}.$$

在聚合物相中, 取 T_1^p , S_2^p , S_3^p , E_3^p 为独立变量, 本构方程可表示为

$$\begin{bmatrix} S_1^p \\ T_2^p \\ T_3^p \\ D_3^p \end{bmatrix} = A^p \times \begin{bmatrix} T_1^p \\ S_2^p \\ S_3^p \\ E_3^p \end{bmatrix}, \quad (9)$$

$$A^p = \begin{bmatrix} \frac{1}{C_{11}^p} & -\frac{C_{12}^p}{C_{11}^p} & -\frac{C_{12}^p}{C_{11}^p} & 0 \\ \frac{C_{12}^p}{C_{11}^p} & C_{11}^p - \frac{C_{12}^p{}^2}{C_{11}^p} & C_{12}^p - \frac{C_{12}^p{}^2}{C_{11}^p} & 0 \\ \frac{C_{12}^p}{C_{11}^p} & C_{12}^p - \frac{C_{12}^p{}^2}{C_{11}^p} & C_{11}^p - \frac{C_{12}^p{}^2}{C_{11}^p} & 0 \\ 0 & 0 & 0 & \varepsilon_{11}^p \end{bmatrix}.$$

在复合材料中, 取 T_1^{cp} , S_2^{cp} , S_3^{cp} , E_3^{cp} 为独立变量, 本构方程可表示为

$$\begin{bmatrix} S_1^{cp} \\ T_2^{cp} \\ T_3^{cp} \\ D_3^{cp} \end{bmatrix} = v_c \begin{bmatrix} S_1^c \\ T_2^c \\ T_3^c \\ D_3^c \end{bmatrix} + v_p \begin{bmatrix} S_1^p \\ T_2^p \\ T_3^p \\ D_3^p \end{bmatrix} = v_c A^c \begin{bmatrix} T_1^c \\ S_2^c \\ S_3^c \\ E_3^c \end{bmatrix} + v_p A^p \times \begin{bmatrix} T_1^p \\ S_2^p \\ S_3^p \\ E_3^p \end{bmatrix} = (v_c A^c + v_p A^p) \times \begin{bmatrix} T_1^{cp} \\ S_2^{cp} \\ S_3^{cp} \\ E_3^{cp} \end{bmatrix}, \quad (10)$$

压电复合材料本构方程可以表示为

$$\begin{bmatrix} T_1^{cp} \\ T_2^{cp} \\ T_3^{cp} \\ D_3^{cp} \end{bmatrix} = \begin{bmatrix} C_{11}^{cp} & C_{12}^{cp} & C_{13}^{cp} & -e_{31}^{cp} \\ C_{12}^{cp} & C_{22}^{cp} & C_{23}^{cp} & -e_{32}^{cp} \\ C_{13}^{cp} & C_{23}^{cp} & C_{33}^{cp} & -e_{33}^{cp} \\ e_{31}^{cp} & e_{32}^{cp} & e_{33}^{cp} & \varepsilon_{33}^{cp} \end{bmatrix} \times \begin{bmatrix} S_1^{cp} \\ S_2^{cp} \\ S_3^{cp} \\ E_3^{cp} \end{bmatrix}, \quad (11)$$

$$\begin{aligned} C_{11}^{cp} &= \frac{C_{11}^c C_{11}^p}{v_c C_{11}^p + v_p C_{11}^c}, \quad C_{12}^{cp} = \frac{v_c C_{12}^c C_{11}^p + v_p C_{12}^p C_{11}^c}{v_c C_{11}^p + v_p C_{11}^c}, \\ C_{13}^{cp} &= \frac{v_c C_{13}^c C_{11}^p + v_p C_{13}^p C_{11}^c}{v_c C_{11}^p + v_p C_{11}^c}, \\ C_{22}^{cp} &= v_c \left(C_{11}^c - \frac{C_{12}^c{}^2}{C_{11}^c} \right) + v_p \left(C_{11}^p - \frac{C_{12}^p{}^2}{C_{11}^p} \right) \\ &\quad + \frac{(v_c C_{12}^c C_{11}^p + v_p C_{12}^p C_{11}^c)^2}{C_{11}^c C_{11}^p (v_c C_{11}^p + v_p C_{11}^c)}, \\ C_{23}^{cp} &= v_c \left(C_{13}^c - \frac{C_{12}^c C_{13}^c}{C_{11}^c} \right) + v_p \left(C_{12}^p - \frac{C_{12}^p{}^2}{C_{11}^p} \right) \\ &\quad + \frac{(v_c C_{13}^c C_{11}^p + v_p C_{13}^p C_{11}^c)(v_c C_{12}^c C_{11}^p + v_p C_{12}^p C_{11}^c)}{C_{11}^c C_{11}^p (v_c C_{11}^p + v_p C_{11}^c)}, \\ C_{33}^{cp} &= v_c \left(C_{33}^c - \frac{C_{13}^c{}^2}{C_{11}^c} \right) + v_p \left(C_{11}^p - \frac{C_{12}^p{}^2}{C_{11}^p} \right) \\ &\quad + \frac{(v_c C_{13}^c C_{11}^p + v_p C_{13}^p C_{11}^c)^2}{C_{11}^c C_{11}^p (v_c C_{11}^p + v_p C_{11}^c)}, \\ e_{31}^{cp} &= \frac{v_c C_{11}^c e_{31}^c}{v_c C_{11}^p + v_p C_{11}^c}, \quad e_{32}^{cp} = v_c \left(e_{31}^c - \frac{C_{12}^c e_{31}^c}{C_{11}^c} \right) \\ &\quad + \frac{v_c e_{31}^c (v_c C_{12}^c C_{11}^p + v_p C_{12}^p C_{11}^c)}{C_{11}^c (v_c C_{11}^p + v_p C_{11}^c)}, \\ e_{33}^{cp} &= v_c \left(e_{33}^c - \frac{C_{13}^c e_{31}^c}{C_{11}^c} \right) + \frac{v_c e_{31}^c (v_c C_{13}^c C_{11}^p + v_p C_{13}^p C_{11}^c)}{C_{11}^c (v_c C_{11}^p + v_p C_{11}^c)}, \\ \varepsilon_{33}^{cp} &= v_c \left(\varepsilon_{33}^c + \frac{e_{31}^c{}^2}{C_{11}^c} \right) + v_p \varepsilon_{11}^p - \frac{v_c^2 C_{11}^p e_{31}^c{}^2}{C_{11}^c (v_c C_{11}^p + v_p C_{11}^c)}. \end{aligned}$$

3 新型径向复合换能器理论推导

3.1 2-2 型压电陶瓷复合材料圆环径向振动的等效电路

图 3 是一个径向极化的压电陶瓷复合材料圆环, 其中 b , c 和 h 分别是圆环内外半径和厚度. 压电本构方程可以表示为

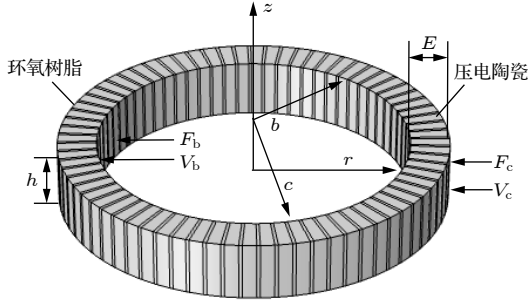


图 3 压电陶瓷复合材料圆环
Fig. 3. Piezoelectric ceramic composite ring.

$$T_\theta = C_{11}^{\text{cp}} S_\theta + C_{12}^{\text{cp}} S_z + C_{13}^{\text{cp}} S_r - e_{31}^{\text{cp}} E_r, \quad (12)$$

$$T_z = C_{12}^{\text{pc}} S_\theta + C_{22}^{\text{pc}} S_z + C_{23}^{\text{pc}} S_r - e_{32}^{\text{pc}} E_r, \quad (13)$$

$$T_r = C_{13}^{\text{cp}} S_\theta + C_{23}^{\text{cp}} S_z + C_{33}^{\text{cp}} S_r - e_{33}^{\text{cp}} E_r, \quad (14)$$

$$D_r = e_{31}^{\text{cp}} S_\theta + e_{32}^{\text{cp}} S_z + e_{33}^{\text{cp}} S_r + \varepsilon_{33}^{\text{cp}} E_r, \quad (15)$$

其中 T_θ , T_z , T_r 分别表示切向应力, 纵向应力和径向应力; S_θ , S_z , S_r 分别表示切向应变, 纵向应变和径向应变; $E_r = E_r(r, t)$ 是径向激励电场; $D_r = D_r(r, t)$ 是电位移矢量; C_{ij}^{cp} , e_{ij}^{cp} , $\varepsilon_{ij}^{\text{cp}}$ 分别代表压电陶瓷复合圆环的等效弹性常数、压电常数以及介电常数. 由于换能器厚度远小于径向尺寸, 因此换能器的振动可以看成平面应力问题^[12], 即 $T_z = 0$. 将 (13) 式变形为

$$S_z = \frac{e_{32}^{\text{cp}} E_r - C_{12}^{\text{cp}} S_\theta - C_{23}^{\text{cp}} S_r}{C_{22}^{\text{pc}}}. \quad (16)$$

将 (16) 式分别代入 (12) 式、(14) 式和 (15) 式得^[13]

$$T_\theta = \left[C_{11}^{\text{cp}} - \frac{(C_{12}^{\text{cp}})^2}{C_{22}^{\text{pc}}} \right] S_\theta + \left(C_{13}^{\text{cp}} - \frac{C_{12}^{\text{cp}} C_{23}^{\text{cp}}}{C_{22}^{\text{pc}}} \right) S_r - \left(e_{31}^{\text{cp}} - \frac{C_{12}^{\text{cp}} e_{32}^{\text{cp}}}{C_{22}^{\text{pc}}} \right) E_r, \quad (17)$$

$$T_r = \left[C_{13}^{\text{cp}} - \frac{C_{12}^{\text{cp}} C_{23}^{\text{cp}}}{C_{22}^{\text{pc}}} \right] S_\theta + \left(C_{33}^{\text{cp}} - \frac{(C_{23}^{\text{cp}})^2}{C_{22}^{\text{pc}}} \right) S_r - \left(e_{33}^{\text{cp}} - \frac{C_{23}^{\text{cp}} e_{32}^{\text{cp}}}{C_{22}^{\text{pc}}} \right) E_r, \quad (18)$$

$$D_r = \left[e_{31}^{\text{cp}} - \frac{e_{32}^{\text{cp}} C_{12}^{\text{cp}}}{C_{22}^{\text{pc}}} \right] S_\theta + \left(e_{33}^{\text{cp}} - \frac{e_{32}^{\text{cp}} C_{23}^{\text{cp}}}{C_{22}^{\text{pc}}} \right) S_r + \left(\varepsilon_{33}^{\text{cp}} - \frac{e_{32}^{\text{cp}} e_{32}^{\text{cp}}}{C_{22}^{\text{pc}}} \right) E_r. \quad (19)$$

压电陶瓷复合材料圆环径向振动的波动方程及应变和位移关系可以表示为

$$\rho \frac{\partial^2 \xi_r}{\partial t^2} = \frac{\partial T_r}{\partial r} + \frac{T_r - T_\theta}{r}, \quad (20)$$

$$S_r = \frac{\partial \xi_r}{\partial r}, \quad S_\theta = \frac{\xi_r}{r}. \quad (21)$$

电场强度幅值可以表示为

$$E_{r0} = B_3 S_\theta + B_5 S_r + \frac{L_3}{r} \frac{C_{22}^{\text{cp}}}{\varepsilon_{33}^{\text{cp}} C_{22}^{\text{cp}} + (e_{32}^{\text{cp}})^2}. \quad (22)$$

式中, L_3 是一个常数, 可由电边界条件决定,

$$B_3 = \frac{e_{32}^{\text{cp}} C_{12}^{\text{cp}} - e_{31}^{\text{cp}} C_{22}^{\text{cp}}}{\varepsilon_{33}^{\text{cp}} C_{22}^{\text{cp}} + (e_{32}^{\text{cp}})^2}, \quad B_5 = \frac{e_{32}^{\text{cp}} C_{23}^{\text{cp}} - e_{33}^{\text{cp}} C_{22}^{\text{cp}}}{\varepsilon_{33}^{\text{cp}} C_{22}^{\text{cp}} + (e_{32}^{\text{cp}})^2}.$$

将 (22) 式代入 (17) 式和 (18) 式得

$$T_\theta = B_1 S_\theta + B_2 S_r + B_3 \frac{L_3}{r}, \quad (23)$$

$$T_r = B_2 S_\theta + B_4 S_r + B_5 \frac{L_3}{r}. \quad (24)$$

式中,

$$B_1 = \left(C_{11}^{\text{cp}} - \frac{C_{12}^{\text{cp}} C_{12}^{\text{cp}}}{C_{22}^{\text{pc}}} \right) - \left(e_{31}^{\text{cp}} - \frac{C_{12}^{\text{cp}} e_{32}^{\text{cp}}}{C_{22}^{\text{pc}}} \right) \times \frac{e_{32}^{\text{cp}} C_{12}^{\text{cp}} - e_{31}^{\text{cp}} C_{22}^{\text{cp}}}{\varepsilon_{33}^{\text{cp}} C_{22}^{\text{cp}} + (e_{32}^{\text{cp}})^2},$$

$$B_2 = \left(C_{13}^{\text{cp}} - \frac{C_{12}^{\text{cp}} C_{23}^{\text{cp}}}{C_{22}^{\text{pc}}} \right) - \left(e_{31}^{\text{cp}} - \frac{C_{12}^{\text{cp}} e_{32}^{\text{cp}}}{C_{22}^{\text{pc}}} \right) \times \frac{e_{32}^{\text{cp}} C_{23}^{\text{cp}} - e_{33}^{\text{cp}} C_{22}^{\text{cp}}}{\varepsilon_{33}^{\text{cp}} C_{22}^{\text{cp}} + (e_{32}^{\text{cp}})^2},$$

$$B_4 = \left(C_{33}^{\text{cp}} - \frac{C_{23}^{\text{cp}} C_{23}^{\text{cp}}}{C_{22}^{\text{pc}}} \right) - \left(e_{33}^{\text{cp}} - \frac{C_{23}^{\text{cp}} e_{32}^{\text{cp}}}{C_{22}^{\text{pc}}} \right) \times \frac{e_{32}^{\text{cp}} C_{23}^{\text{cp}} - e_{33}^{\text{cp}} C_{22}^{\text{cp}}}{\varepsilon_{33}^{\text{cp}} C_{22}^{\text{cp}} + (e_{32}^{\text{cp}})^2}.$$

将 (21) 式、(23) 式和 (24) 式代入 (20) 式并分离时间变量得

$$\frac{d^2 \xi_{r0}}{dr^2} + \frac{1}{r} \frac{d \xi_{r0}}{dr} + (k^2 - \frac{v^2}{r^2}) \xi_{r0} - B'_3 \frac{L_3}{r^2} = 0, \quad (25)$$

式中,

$$v^2 = B_1/B_4, \quad B'_3 = B_1/B_3, \quad k = \omega/V_3,$$

$$V_3^2 = B_4/\rho, \quad \rho = v_c \rho_c + v_p \rho_p,$$

ω 是角频率, ρ , ρ_c 和 ρ_p 分别是压电复合材料等效密度, 压电相密度和聚合物相密度, k 和 V_3 分别是波数和径向极化压电陶瓷复合材料圆环中径向振动的传播速度. 方程 (25) 是广义贝塞尔方程, 其解为

$$\xi_{r0} = A_1 J_v(kr) + A_2 Y_v(kr) + B'_3 L_3 s_{-1,v}(kr), \quad (26)$$

式中, $J_v(kr)$, $Y_v(kr)$ 是 v 阶的第一类和第二类贝塞尔函数, $s_{-1,v}(kr)$ 是第一类隆梅尔函数, A_1 , A_2 是两个常数. 根据 (26) 式可以得出径向振动压电陶瓷复合材料圆环的径向振动速度为

$$v_{r0} = j\omega[A_1 J_v(kr) + A_2 Y_v(kr) + B'_3 L_3 s_{-1,v}(kr)]. \quad (27)$$

根据速度边界条件: $v|_{r=b} = v_b$, $v|_{r=c} = -v_c$ 可得

$$A_1 = -\frac{jY_v(kc)}{\omega\tau_1}v_b - \frac{jY_v(kb)}{\omega\tau_1}v_c + \frac{\tau_2}{\tau_1}L_3, \quad (28)$$

$$A_2 = \frac{jY_v(kc)}{\omega\tau_1}v_b + \frac{jY_v(kb)}{\omega\tau_1}v_c + \frac{\tau_3}{\tau_1}L_3. \quad (29)$$

式中, τ_1 , τ_2 和 τ_3 是三个引入的常数, 其具体表达式为

$$\tau_1 = J_v(kb)Y_v(kc) - J_v(kc)Y_v(kb),$$

$$\tau_2 = B'_3[Y_v(kb)s_{-1,v}(kc) - Y_v(kc)s_{-1,v}(kb)],$$

$$\tau_3 = B'_3[J_v(kc)s_{-1,v}(kb) - J_v(kb)s_{-1,v}(kc)].$$

压电复合陶瓷圆环内外表面间的电压可表示为

$$V_{r0} = -\int_b^c E_{r0} dr = -\frac{jkbX_b}{\omega}v_b - \frac{jkcX_c}{\omega}v_c - \frac{L_3 P}{\tau_1}. \quad (30)$$

式中,

$$X_b = B_3 \left\{ (v-2)s_{-2,v-1}(kb) - \frac{[J_{v-1}(kb)Y_v(kc) - J_v(kc)Y_{v-1}(kb)]s_{-1,v}(kb)}{\tau_1} - \frac{2s_{-1,v}(kc)}{\pi kb\tau_1} \right\} + \frac{B_5}{kb},$$

$$X_c = B_3 \left\{ (v-2)s_{-2,v-1}(kc) + \frac{[J_{v-1}(kc)Y_v(kb) - J_v(kb)Y_{v-1}(kc)]s_{-1,v}(kc)}{\tau_1} + \frac{2s_{-1,v}(kb)}{\pi kc\tau_1} \right\} + \frac{B_5}{kc},$$

$$P = \tau_1 \left\{ \frac{B_3 B'_3 (H_c - H_b)}{2v^2(4-v^2)} + B_5 B'_3 [s_{-1,v}(kc) - s_{-1,v}(kb)] + \left(\frac{C_{22}^{cp}}{\epsilon_{33}^{cp} C_{22}^{cp} + e_{32}^{cp} e_{32}^{cp}} - \frac{B_3 B'_3}{v^2} \right) (\ln c - \ln b) \right\} \\ + \tau_2 \{ B_3 [(v-2)(J_{1c} - J_{1b}) + J_{2b} - J_{2c}] + B_5 [J_v(kc) - J_v(kb)] \} \\ + \tau_3 \{ B_3 [(v-2)(Y_{1c} - Y_{1b}) + Y_{2b} - Y_{2c}] + B_5 [Y_v(kc) - Y_v(kb)] \},$$

$$J_{1r} = kr J_v(kr) s_{-2,v-1}(kr),$$

$$J_{2r} = kr J_{v-1}(kr) s_{-1,v}(kr),$$

$$Y_{1r} = kr Y_v(kr) s_{-2,v-1}(kr),$$

$$Y_{2r} = kr Y_{v-1}(kr) s_{-1,v}(kr),$$

$$H_r = (kr)^2 {}_2F_3 \left([1, 1], \left[2, 2 + \frac{1}{2}v, 2 - \frac{1}{2}v \right], -\frac{1}{4}(kr)^2 \right).$$

根据压电复合陶瓷径向力边界条件: $F_b = -T_b S_b$, $F_c = -T_c S_c$, 其中 $S_b = 2\pi b h$, $S_c = 2\pi c h$, 化简可得

$$F'_b = cX_c F_b = \left\{ -\frac{n^2}{j\omega C_0} - Z_b \frac{j c^2 X_c^2 [J_v(kc)Y_{v-1}(kb) - J_{v-1}(kb)Y_v(kc)]}{\tau_1} \right. \\ \left. + \frac{4j\pi h c^2 X_c^2 (B_2 - B_4 v)}{\omega} \right\} v'_b \\ + \left(-\frac{n^2}{j\omega C_0} - Z_b \frac{2j b X_c M_b}{\pi k \tau_1} \right) v'_c + nV_{r0}, \quad (31)$$

$$F'_c = bX_b F_c = \left\{ -\frac{n^2}{j\omega C_0} - Z_c \frac{j b^2 X_b^2 [J_v(kb)Y_{v-1}(kc) - J_{v-1}(kc)Y_v(kb)]}{\tau_1} \right. \\ \left. + \frac{4j\pi h b^2 X_b^2 (B_4 v - B_2)}{\omega} \right\} v'_c \\ + \left(-\frac{n^2}{j\omega C_0} - Z_c \frac{2j c X_c M_b}{\pi k \tau_1} \right) v'_b + nV_{r0}. \quad (32)$$

式中,

$$Z_b = \frac{kB_4 S_b}{\omega} = \rho V_3 S_b, \quad Z_c = \frac{kB_4 S_c}{\omega} = \rho V_3 S_c,$$

$$n_1 = cX_c, \quad n_2 = bX_b,$$

$$v'_b = \frac{v_b}{n_2}, \quad v'_c = \frac{v_c}{n_1}, \quad n = 2\pi h \tau_1 k b c X_b X_c / P,$$

$$C_0 = 2\pi h \tau_1 / P,$$

n 和 C_0 分别是机电转换系数和钳定电容. 流过压电陶瓷复合材料圆环的电流可以由下式得出:

$$I_r = -\frac{dQ}{dt} = -j\omega \int_{-h/2}^{h/2} \int_0^{2\pi} L_3 d\theta dz = -j\omega 2\pi h L_3 \\ = -n(v'_b + v'_c) + j\omega C_0 V_{r0}. \quad (33)$$

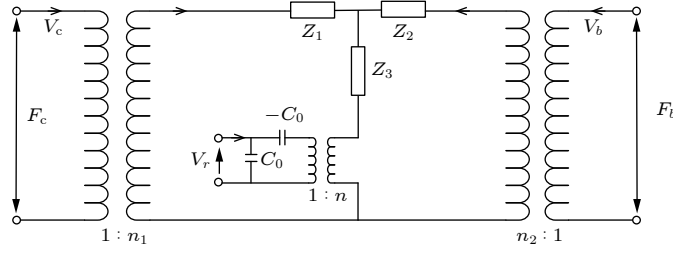


图 4 径向极化压电陶瓷复合圆环径向振动的机电等效电路

Fig. 4. Electromechanical equivalent circuit of radial vibration of a piezoelectric ceramic composite ring with radial polarization.

基于以上推导,可以得到径向极化压电陶瓷复合材料圆环径向振动的六端机电等效电路如图 4 所示.

图 4 中,各个部分阻抗的表达式如下:

$$Z_1 = -Z_b \frac{j c^2 X_c^2 [J_v(kc) Y_{v-1}(kb) - J_{v-1}(kb) Y_v(kc)]}{\tau_1} + \frac{2j\pi h c^2 X_c^2 (B_2 - B_4 v)}{\omega} + Z_b \frac{2j c X_c X_b}{\pi k \tau_1}, \quad (34)$$

$$Z_2 = -Z_c \frac{j b^2 X_b^2 [J_v(kb) Y_{v-1}(kc) - J_{v-1}(kc) Y_v(kb)]}{\tau_1} + \frac{2j\pi h b^2 X_b^2 (B_4 v - B_2)}{\omega} + Z_c \frac{2j b X_c X_b}{\pi k \tau_1}, \quad (35)$$

$$Z_3 = -Z_b \frac{2j c X_c X_b}{\pi k \tau_1} = -Z_c \frac{2j b X_c X_b}{\pi k \tau_1}. \quad (36)$$

3.2 金属圆环径向振动的等效电路

金属圆环内外半径,厚度分别为 \$a, b, h\$,其径向振动的四端机电等效电路如图 5 所示.

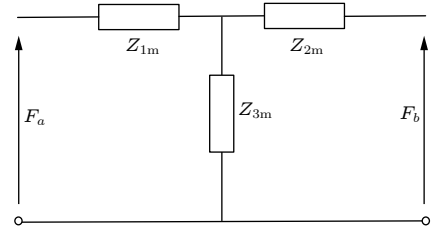


图 5 径向振动金属圆环的机电等效电路

Fig. 5. Electromechanical equivalent circuit of radial vibration of metal ring.

在图 5 中,各个阻抗的表达式如下 [13]:

$$Z_{1m} = j \frac{2Z_{0a}}{\pi k_0 a [J_1(k_0 b) Y_1(k_0 a) - J_1(k_0 a) Y_1(k_0 b)]} \times \frac{J_1(k_0 b) Y_0(k_0 a) - J_0(k_0 a) Y_1(k_0 b) - J_1(k_0 a) Y_0(k_0 a) + J_0(k_0 a) Y_1(k_0 a)}{J_1(k_0 a) Y_0(k_0 a) - J_0(k_0 a) Y_1(k_0 a)} - j \frac{2Z_{0a}(1-v_0)}{\pi(k_0 a)^2 [J_1(k_0 a) Y_0(k_0 a) - J_0(k_0 a) Y_1(k_0 a)]}, \quad (37)$$

$$Z_{2m} = j \frac{2Z_{0a}}{\pi k_0 a [J_1(k_0 b) Y_1(k_0 a) - J_1(k_0 a) Y_1(k_0 b)]} \times \frac{J_1(k_0 a) Y_0(k_0 b) - J_0(k_0 b) Y_1(k_0 a) - J_1(k_0 b) Y_0(k_0 b) + J_0(k_0 b) Y_1(k_0 a)}{J_1(k_0 b) Y_0(k_0 b) - J_0(k_0 b) Y_1(k_0 b)} + j \frac{2Z_{0b}(1-v_0)}{\pi(k_0 b)^2 [J_1(k_0 b) Y_0(k_0 b) - J_0(k_0 b) Y_1(k_0 b)]}, \quad (38)$$

$$Z_{3m} = \frac{-2jZ_{0a}}{k_0 a \pi [J_1(k_0 b) Y_1(k_0 a) - J_1(k_0 a) Y_1(k_0 b)]} = \frac{-2jZ_{0b}}{k_0 b \pi [J_1(k_0 a) Y_1(k_0 b) - J_1(k_0 b) Y_1(k_0 a)]}. \quad (39)$$

式中,

$$S_a = 2\pi a h, S_b = 2\pi b h, Z_{0a} = \rho_0 v_r S_a, Z_{0b} = \rho_0 v_r S_b, k_0 = \omega/v_r, v_r^2 = \frac{E_0}{\rho_0(1-v_0^2)},$$

\$\rho_0, E_0\$ 和 \$v_0\$ 分别是金属圆环的密度、杨氏模量和泊松比, \$k_0\$ 和 \$v_r\$ 分别是金属圆环中波数和径向振动的传播速度.

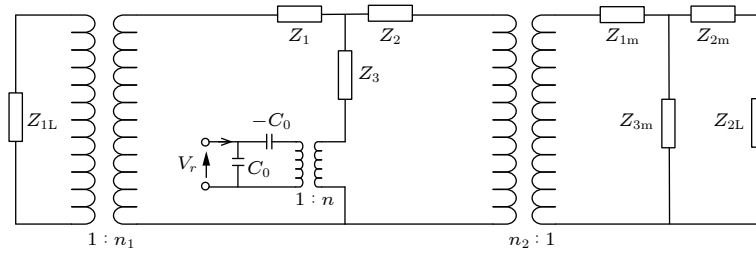


图6 径向振动压电陶瓷复合材料圆环换能器的机电等效电路

Fig. 6. Electromechanical equivalent circuit of radial vibration piezoelectric ceramic composite toroidal transducer.

3.3 新型径向复合换能器的等效电路及频率方程

利用力及振速的连续性条件, 可以得出径向振动压电陶瓷复合材料圆环换能器的机电等效电路, 如图6所示.

图6中 Z_{1L} 和 Z_{2L} 分别代表新型换能器内外表面的径向负载阻抗, 当忽略换能器内外负载阻抗, 即 Z_{1L} 和 Z_{2L} 都为0时, 由图6可以得到整个换能器的机械阻抗为^[14]

$$Z_m = Z_3 + \frac{Z_1(Z_2 + n_2^2 Z_{om})}{Z_1 + Z_2 + n_2^2 Z_{om}}, \quad (40)$$

其中压电复合陶瓷圆环机械阻抗为

$$Z_{om} = Z_{1m} + \frac{Z_{2m} Z_{3m}}{Z_{2m} + Z_{3m}}, \quad (41)$$

换能器的输入电阻抗为

$$Z_e = \frac{V}{I} = \frac{n^2 - j\omega C_0 Z_m}{\omega^2 C_0^2 Z_m}, \quad (42)$$

则换能器共振频率方程为

$$n^2 - j\omega C_0 Z_m = 0, \quad (43)$$

反共振频率方程为

$$\omega^2 C_0^2 Z_m = 0. \quad (44)$$

4 换能器振动性能分析

4.1 换能器振动性能与几何尺寸、两相体积占比的关系

通过求解频率方程(43)式和(44)式可以得出换能器的共振及反共振频率, 从而可以对换能器的共振频率与其几何尺寸^[15]以及复合材料两相体积占比^[16]之间的关系进行进一步的研究. 金属圆环的材料为不锈钢, 其材料参数为^[4]

$\rho_0 = 7800 \text{ kg/m}^3$, $E = 2.09 \times 10^{11} \text{ N/m}^2$, $\nu_0 = 0.28$.

压电陶瓷复合材料圆环的压电相为PZT-4, 其

材料参数为

$\rho_c = 7500 \text{ kg/m}^3$, $C_{11}^c = 13.9 \times 10^{10} \text{ N/m}^2$, $C_{12}^c = 7.78 \times 10^{10} \text{ N/m}^2$, $C_{13}^c = 7.43 \times 10^{10} \text{ N/m}^2$, $C_{33}^c = 11.5 \times 10^{10} \text{ N/m}^2$, $e_{31}^c = -5.2 \text{ Nm/V}$, $e_{33}^c = 15.1 \text{ Nm/V}$, $\epsilon_{33}^c = 5.62 \text{ C/m}$.

聚合物相为环氧树脂, 其材料参数为^[17]:

$\rho_0 = 1050 \text{ kg/m}^3$, $C_{11}^p = 8 \times 10^{10} \text{ N/m}^2$, $C_{12}^p = 4.4 \times 10^{10} \text{ N/m}^2$, $\epsilon_{11}^p = 0.037 \times 10^{-9} \text{ C/m}$.

换能器的几何尺寸分别为: $a = 6 \text{ mm}$, $c = 26 \text{ mm}$, $h = 6 \text{ mm}$, $a \leq b \leq c$.

图7(a)和图7(b)是换能器一阶共振频率和反共振频率与其半径比 $\tau = \frac{b-a}{c-a}$ 之间的理论关系. 如图7(a)所示, 同一两相体积占比($v_p/v_c = 0.25$)情况下, 当半径比增加时, 新型复合换能器的一阶共振频率和反共振频率呈下降趋势. 用 f_r , f_a 分别表示换能器的共振频率和反共振频率, 换能器有效机电耦合系数可以表示为 $k_{\text{eff}} = \sqrt{1 - (f_r/f_a)^2}$. 如图7(b)所示, 同一两相占比($v_p/v_c = 0.25$)情况下, 当半径比增加时, 新型复合换能器的有效机电耦合系数呈先增大后减小的趋势, 半径比在0.35左右, 有效机电耦合系数取到最大值. 另外, 如图7(c)和图7(d)所示, 同一半径比($\tau = 0.6$)情况下, 当两相占比增加时, 新型复合换能器的一阶共振频率和反共振频率呈上升趋势, 而有效机电耦合系数呈下降趋势. 因此在实际换能器设计中, 应充分考虑尺寸与两相占比对换能器振动性能的影响, 为了得到较高的机电转换效率, 换能器半径比设计应尽量接近于0.35, 聚合物相占比越高虽然会导致机电转换效率降低, 但同时也能带来更好的声匹配能力, 因此在换能器设计中选择较低聚合物相占比即可.

4.2 换能器振动性能的仿真模拟

为验证换能器的解析理论, 利用仿真软件(CO-MSOOL Multiphysics 5.4)对换能器的振动模态及

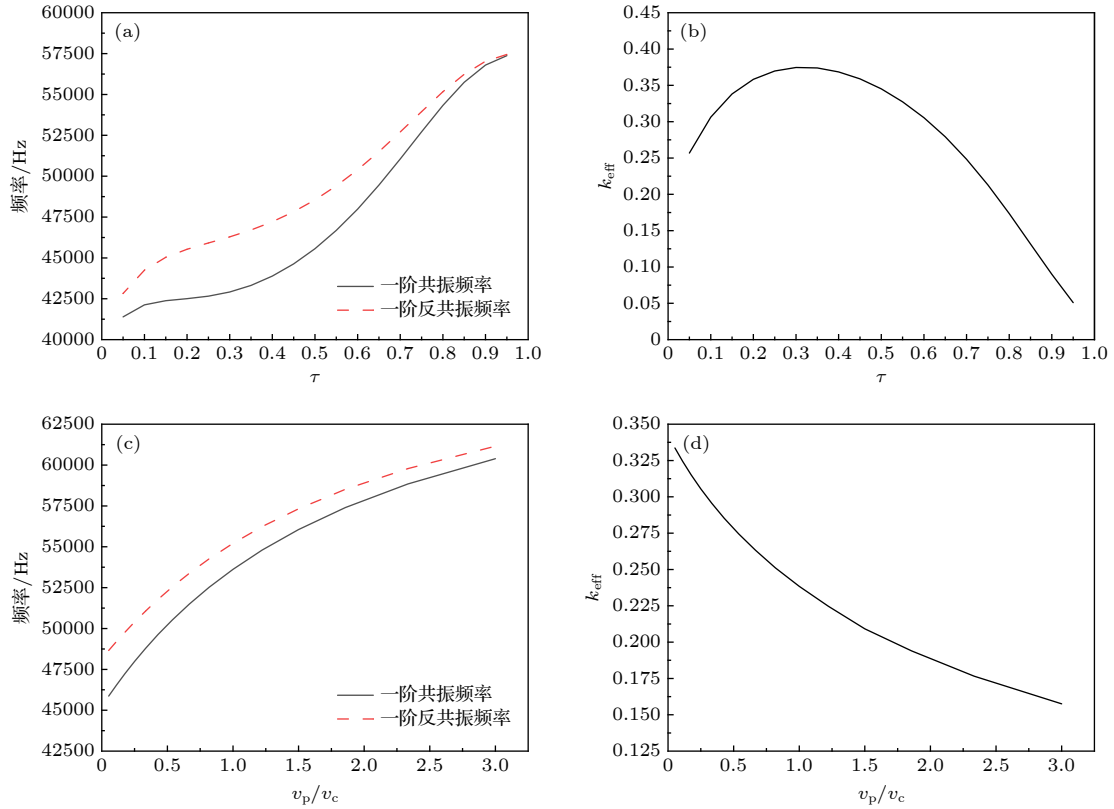


图 7 (a) 换能器的一阶共振频率和反共振频率与几何尺寸之间的关系; (b) 换能器的有效机电耦合系数与几何尺寸之间的关系; (c) 换能器的一阶共振频率和反共振频率与两相占比之间的关系; (d) 换能器的有效机电耦合系数与两相占比之间的关系

Fig. 7. (a) Relationship between the first-order resonance frequency and anti-resonance frequency of the transducer and the geometrical size; (b) relationship between the effective electromechanical coupling coefficient and geometric dimensions of the transducer; (c) relationship between the first-order resonance frequency and anti-resonance frequency of the transducer and the proportion of the two phases; (d) relationship between the effective electromechanical coupling coefficient of the transducer and the proportion of the two phases.

共振频率进行了数值模拟. 结果如表 1 所示, f_r , f_a 分别表示换能器一阶径向振动共振频率、反共振频率的理论计算结果, f_{r1} , f_{a1} 分别表示换能器一阶径向振动数值模拟结果, 误差 $A_1 = |f_r - f_{r1}|/f_{r1}$, $A_2 = |f_a - f_{a1}|/f_{a1}$. 而误差主要来源于在解析理论中, 假设换能器的厚度远小于其径向尺寸, 理想情况应该是无限小, 而在数值模拟过程中换能器尺寸则是有限的, 此外在复合材料等效参数推导中并没有考虑材料形状对结构参数的影响, 因此会产生一定误差. 由表 1 可以看出, 数值模拟得到的换能器在不同半径比或不同两相占比的情况下 (空气中), 一阶径向振动的共振频率、反共振频率与根据解析法得出的结果吻合较好, 从而验证了新型换能器理论设计的正确性, 图 8 为表 1 不同半径比或不同两相占比的换能器共振时的振动模态图像.

4.3 相比传统径向换能器的性能提升

为了验证新型换能器相比传统径向换能器的

性能提升, 利用仿真软件 (COMSOL Multiphysics 5.4) 对换能器在水下的辐射声场进行了仿真研究^[18], 假设换能器处在无限大水域内工作. 在 53 到 65 kHz 范围内, 同一尺寸 ($a=6$ mm, $b=16$ mm, $c=24$ mm, $h=6$ mm, $v_p/v_c=0.429$) 的新型换能器的发射电压响应相比传统径向换能器幅值更大, 其原因在于采用压电复合材料以后, 换能器的声阻抗匹配得到了改善. 另外, 以中心频率对应发射电压响应左右下降 3 dB 取换能器工作带宽^[19,20], 由数值模拟结果可知该尺寸下新型径向换能器在水中振动的中心频率在 53082 Hz, 振动模态如图 9(a) 所示, 传统径向换能器的中心频率在 55356 Hz, 振动模态如图 9(c) 所示, 则由图 10 可见, 新型换能器工作带宽为 6000 Hz 左右, 即为图 10 中两蓝线间隔, 而传统径向换能器工作带宽为 3000 Hz 左右, 即为图 10 中两绿线间隔, 两者相差接近一倍, 因此新型换能器相比传统径向换能器性能上有

表 1 新型径向复合材料换能器共振频率的理论及数值模拟结果 (一阶径向振动)

Table 1. Theoretical and numerical simulation results of the resonance frequency of the new radial composite transducer (first-order radial vibration).

a/mm	b/mm	c/mm	v_p/v_c	h/mm	f_r/Hz	f_a/Hz	f_{r1}/Hz	f_{a1}/Hz	$A_1/\%$	$A_2/\%$
6	16	24	0.429	6	51780.7	54216.2	53198.0	53941.0	2.66	3.08
8	16	24	0.429	6	47428.9	49485.3	47552.0	47741.0	2.59	3.65
6	16	24	0.250	6	50047.0	52761.2	52675.0	52941.0	4.99	0.34
8	16	24	0.250	6	45949.4	48257.8	47901.0	48299.0	4.07	0.08

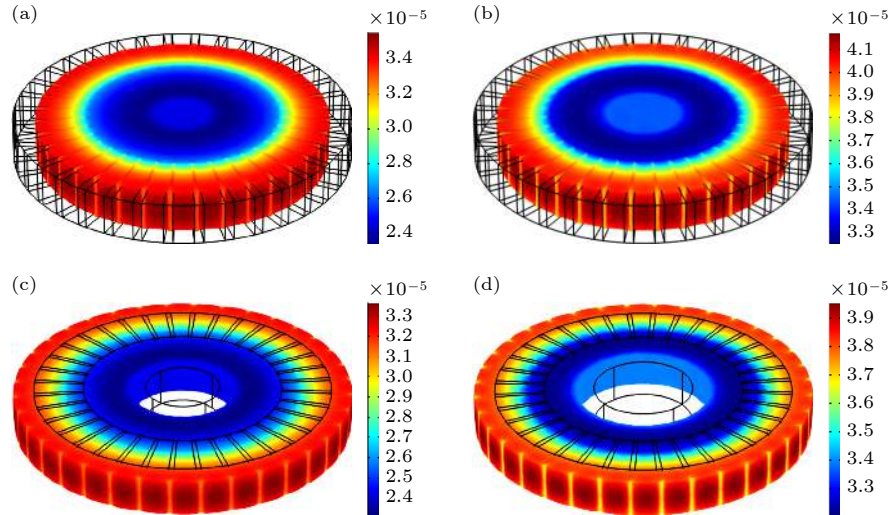


图 8 (a) 换能器共振频率为 53198 Hz 时的振动模式; (b) 换能器共振频率为 47552 Hz 时的振动模式; (c) 换能器共振频率为 52675 Hz 时的振动模式; (d) 换能器共振频率为 47901 Hz 时的振动模式

Fig. 8. (a) The vibration mode of the transducer when the resonance frequency is 53198 Hz; (b) the vibration mode of the transducer when the resonance frequency is 47552 Hz; (c) the vibration mode of the transducer when the resonance frequency is 52675 Hz; (d) the vibration mode of the transducer when the resonance frequency is 47901 Hz.

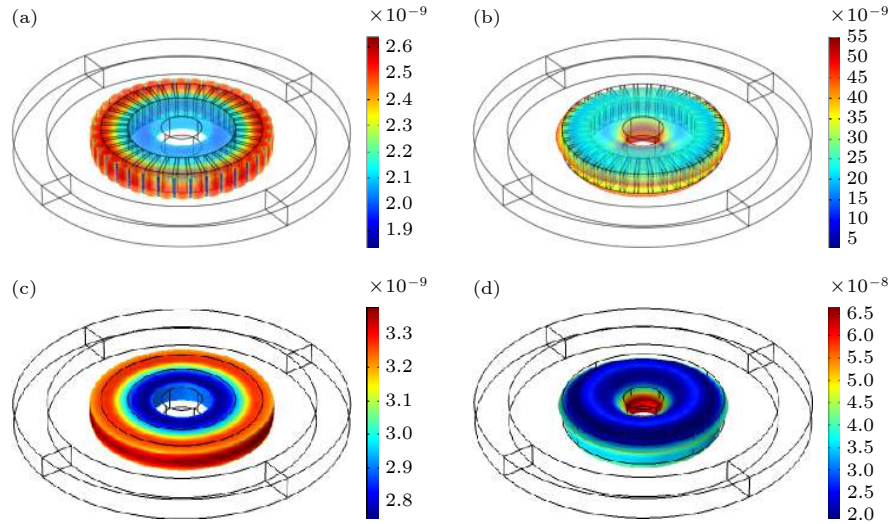


图 9 (a) 换能器共振频率为 53082 Hz 时的振动模式; (b) 换能器共振频率为 68070 Hz 时的振动模式; (c) 换能器共振频率为 55356 Hz 时的振动模式; (d) 换能器共振频率为 73747 Hz 时的振动模式

Fig. 9. (a) The vibration mode of the transducer when the resonance frequency is 53082 Hz; (b) the vibration mode of the transducer when the resonance frequency is 68070 Hz; (c) the vibration mode of the transducer when the resonance frequency is 55356 Hz; (d) the vibration mode of the transducer when the resonance frequency is 73747 Hz.

很大的提升, 是一种针对传统换能器性能提升的改进方案. 另外在图 10 中可以看到新型换能器和传统换能器在 68 和 73 kHz 左右出现峰值, 因此对利用仿真软件对两种换能器在对应峰值频率附近寻找特征频率, 其振动模式分别如图 9(b) 和图 9(d) 所示, 由图可见此时两种换能器的振动模式非常复杂, 存在径向振动和弯曲振动的耦合振动, 且振动位移较大, 因此在水中发射电压响应出现了一个峰值, 但由于振动模式复杂, 并非本文所研究模式.

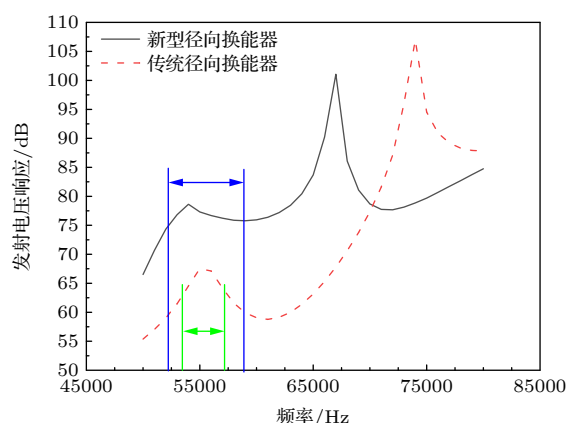


图 10 新型复合材料径向换能器与传统纯陶瓷径向换能器的发射电压响应曲线

Fig. 10. The emission voltage response curves of the new radial transducer and the traditional radial transducer.

5 结 论

本文研究了一种新型径向振动压电陶瓷复合材料圆环换能器, 推导了 2-2 型压电复合材料的等效参数, 得到了径向极化压电陶瓷复合材料圆环换能器的机电等效电路及其频率方程. 利用仿真软件对换能器的径向振动性能进行了数值模拟, 结果表明数值模拟得到的换能器一阶径向振动的共振频率、反共振频率与用解析法得出的结果吻合较好. 主要结论主要有以下几点:

1) 推导了 2-2 型压电复合材料的等效参数, 并将其应用于径向换能器理论设计中;

2) 同一两相占比 ($v_p/v_c = 0.25$) 情况下, 当半径比增加时, 新型复合换能器的一阶共振频率和反共振频率呈下降趋势. 同一两相占比 ($v_p/v_c = 0.25$) 情况下, 当半径比增加时, 复合换能器的有效机电耦合系数呈先增大后减小的趋势, 半径比在 0.35

左右, 有效机电耦合系数取到最大值. 另外, 同一半径比 ($\tau = 0.6$) 情况下, 当两相占比增加时, 复合换能器的一阶共振频率和反共振频率呈上升趋势, 而有效机电耦合系数呈下降趋势;

3) 在 53 到 65 kHz 范围内, 新型复合材料径向换能器相比传统纯陶瓷径向换能器, 发射电压响应幅值更大, 工作带宽提高接近一倍, 声匹配更佳.

参考文献

- [1] Liu S Q, Ma L L 2020 *J. Shaanxi Normal Univ. (Nat. Sci. Ed.)* **48** 60 (in Chinese) [刘世清, 麻磊磊 2020 陕西师范大学学报 (自然科学版) **48** 60]
- [2] Lu D M 2001 *Principle of Underwater Acoustic Transducer* (Qingdao: Qingdao Ocean University Press) pp347–353 (in Chinese) [路德明 2001 水声换能器原理(青岛: 青岛海洋大学出版社) 第347—353页]
- [3] Liang Z F, Mo X P, Zhou G P 2011 *Acta Acustica* **36** 369 (in Chinese) [梁召峰, 莫喜平, 周光平 2011 声学学报 **36** 369]
- [4] Lin S Y 2007 *J. Shaanxi Normal Univ. (Nat. Sci. Ed.)* **35** 254 (in Chinese) [林书玉 2007 陕西师范大学学报 (自然科学版) **35** 254]
- [5] Lin S Y 2008 *Tech. Acoust.* **27** 605 (in Chinese) [林书玉 2008 声学技术 **27** 605]
- [6] Lin S Y 2004 *The Principle And Design Of Ultrasonic Transducer* (Beijing: Science Press) p15 (in Chinese) [林书玉 2004 超声换能器的原理及设计 (北京: 科学出版社) 第15页]
- [7] Xue S 2015 *M. S. Thesis* (Xian: Xidian University) (in Chinese) [薛术 2015 硕士学位论文 (西安: 西安电子科技大学)]
- [8] Smith W A 1991 *IEEE Trans. Ultrason. Ferroelectr. Freq. Control* **38** 40
- [9] Smith W A 1990 *IEEE 1990 Ultrasonics Symposium* Honolulu, HI, December 4–7, 1990 pp757–761
- [10] Newnham R E, Skinner D P, Crossden L E 1978 *Mater. Res. Bull.* **13** 525
- [11] Chen P, Shen Y P, Tian X G 2006 *Chin. Q. Mech.* **1** 29 (in Chinese) [陈鹏, 沈亚鹏, 田晓耕 2006 力学季刊 **1** 29]
- [12] Lin S Y, Wang S J, Fu Z Q, Hu J, Wang C H, Mo R Y 2013 *Acta Acustica* **38** 354 (in Chinese) [林书玉, 王帅军, 付志强, 胡静, 王成会, 莫润阳 2013 声学学报 **38** 354]
- [13] Lin S Y, Fu Z Q, Zhang X L, Wang Y, Hu J 2012 *Smart. Mater. Struct.* **22** 015005
- [14] Wang S J, Lin S Y 2011 *J. Shaanxi Normal Univ. (Nat. Sci. Ed.)* **39** 23 (in Chinese) [王帅军, 林书玉 2011 陕西师范大学学报(自然科学版) **39** 23]
- [15] Lin S Y 2008 *Sens. Actuator, A* **141** 136
- [16] Li Z C 2008 *M. S. Thesis* (Xian: Shaanxi Normal University) (in Chinese) [李争彩 2008 硕士学位论文 (西安: 陕西师范大学)]
- [17] Poizat C H, Sester M 1999 *Comput. Mater. Sci.* **16** 89
- [18] Qing L 2010 *Ph. D. Dissertation* (Beijing: Beijing University of Posts and Telecommunications) (in Chinese) [秦雷 2010 博士学位论文 (北京: 北京邮电大学)]
- [19] Zhong C 2019 *Ph. D. Dissertation* (Beijing: Beijing University of Posts and Telecommunications) (in Chinese) [仲超 2019 博士学位论文 (北京: 北京邮电大学)]
- [20] Wang S, Lin S Y 2019 *Acta Phys. Sin.* **68** 024303 (in Chinese) [王莎, 林书玉 2019 物理学报 **68** 024303]

A new broadband radial vibration ultrasonic transducer based on 2-2 piezoelectric composite material*

Chen Cheng Lin Shu-Yu[†]

(*Shaanxi Key Laboratory of Ultrasonics, Institute of Applied Acoustics, Shaanxi Normal University, Xi'an 710119, China*)

(Received 17 August 2020; revised manuscript received 3 September 2020)

Abstract

Radial vibration transducer has the advantages of large radiation area, high radiation efficiency, uniform radial radiation, and wide range of action. Therefore, it is widely used in the technical fields of ultrasonic liquid treatment such as underwater acoustics, ultrasonic degradation and sonochemistry. On the other hand, the 2-2 piezoelectric composite material is one of the most commonly researched piezoelectric composite materials with the best development prospects. Compared with traditional pure piezoelectric ceramics, this new type of material has the advantages of low impedance, low mechanical quality factor, and frequency bandwidth. Therefore, in this paper we propose a new broadband radial vibration ultrasonic transducer based on 2-2 piezoelectric composite material, which is mainly composed of an inner metal ring and an outer piezoelectric ceramic composite ring. First, the Newnham series-parallel theory and the uniform field theory are used to derive the equivalent parameters of the 2-2 piezoelectric composite material. Second, the radial vibration of the combination of the metal ring and the radially polarized piezoelectric composite ceramic ring are analyzed by the analytical method. The six-terminal electromechanical equivalent circuit of the transducer is obtained, and the frequency equation of the transducer is also obtained. And then the relationship between the resonant frequency and anti-resonant frequency of the transducer, as well as the effective electromechanical coupling coefficient, geometric size, and two-phase volume ratio are analyzed. It is concluded that in order to obtain higher electromechanical conversion efficiency, the design of the transducer radius ratio should be as close as possible to 0.35. Although the higher proportion of polymer phase will lead the electromechanical conversion efficiency to decrease, it can also bring better acoustic matching ability. Therefore, the lower proportion of polymer phase can be selected in the transducer design. The finite element method is used to numerically simulate the radial vibration of the new transducer. The results show that the resonance frequency and anti-resonance frequency obtained by the analytical method are in good agreement with the numerical simulation results. In addition, the acoustic field of the transducer under water is simulated numerically. The results show that compared with the traditional pure ceramic radial transducer, the new composite radial transducer has a large emission voltage response amplitude, the working bandwidth is nearly doubled, and the acoustic matching is better.

Keywords: composite material equivalent parameters, radial vibration, bandwidth, acoustic matching

PACS: 77.84.Lf, 43.38.+n, 43.30.+m

DOI: 10.7498/aps.70.20201352

* Project supported by the National Natural Science Foundation of China (Grant Nos. 11674206, 11874253).

[†] Corresponding author. E-mail: sylin@snnu.edu.cn